Analytical Study of Open-ended Winding Induction Machines Supplied by Fuel Cells and Batteries for Hydrogen Trains

Goren, Hakime Hanife; Tricoli, Pietro

Analytical Study of Open-ended Winding Induction Machines Supplied by Fuel Cells and Batteries for Hydrogen Trains

Hakime Hanife Goren
Department of Electronic, Electrical and Systems Engineering
University of Birmingham
Birmingham, UK
hxg793@student.bham.ac.uk

Pietro Tricoli, *Senior Member*, *IEEE*
Department of Electronic, Electrical and Systems Engineering
University of Birmingham
Birmingham, UK
p.tricoli@bham.ac.uk

***Abstract*—This paper focuses on a new traction system for hydrogen trains supplied by fuel cells and batteries for non-electrified lines. In this topology, the DC/DC converters of the fuel cell and the battery are removed and the motor is fed with open windings from 2 inverters, one for the fuel cell and the other for the battery. The main objective of this study is to understand analytically the main advantages obtained in terms of reduction of the total apparent power of the converters used in the traction systems and evaluate theoretically the constraints on the voltage and current of the 2 inverters.**

Keywords—Open-ended winding induction machines, fuel cells, batteries, traction systems

I. INTRODUCTION

Alternative propulsion systems and energy sources for railway vehicles are currently being investigated by many researchers to reduce carbon emissions. Replacement of diesel with hydrogen for railway vehicles has the potential to reduce emissions considerably when the entire well-to-wheel process is taken into account [1],[2] without the need to electrify the line, which is often not economical for branch lines. Hybrid electric vehicles with hydrogen fuel cells and electric energy storage are promising solutions to optimise the design of the power sources, improve fuel efficiency, and reduce pollutant emissions. The design of the propulsion system of a railway vehicle depends on several factors such as the number of stops, frequency of service, and length of the line [3]. For shorter distances, battery-only trains have an advantage in terms of efficiency and complexity of the power train; however, for larger ranges, only carbon-free fuels like hydrogen can provide the required energy density without emissions [4].

Hydrogen trains are classified with respect to onboard energy storage: fuel cell and batteries; fuel cell and supercapacitors; and fuel cell, batteries, and supercapacitors. The addition of an energy storage system reduces the peak power of the fuel cell stack with significant cost savings [5]. Fuel cells and supercapacitors have found application in the automotive sector, but the low energy density in comparison to batteries prevents any practical railway use, as often trains are required to travel at high speeds for long distances without frequent stops. Therefore, the majority of the research studies have focussed on fuel cells and batteries. For the latter, different types of battery cells have been studied, from lithium nickel manganese cobalt oxides, preferred for their high energy density, to lithium-titanium oxide, preferred for their longer lifetime. Hydrogen trains are also classified on the basis of the fuel stored on the train: indirect power systems mainly use hydrogen from methane steam reforming, while direct power systems use pure hydrogen [6], [7]. The power train can also be based on a single power conversion stage or a double stage. In the first case, the fuel cells feed the traction inverter directly. Conversely, in the two-stage power conversion, shown in Fig. 1, the fuel cell voltage is increased by a boost DC-DC power converter and feeds the traction inverter via a regulated DC-bus. The DC-DC converter is typically interleaved unidirectional, as shown in Fig. 2, to reduce the voltage ripple and the current ratings of semiconductor devices [8] and avoid negative current circulation through the fuel cell that may damage the circuit. Batteries are also connected to the regulated DC bus via an interleaved boost bi-directional DC-DC converter [9], shown in Fig. 3, to enable charging and discharging of the energy storage. However, a double-stage power conversion can be bulky due to the significant weight

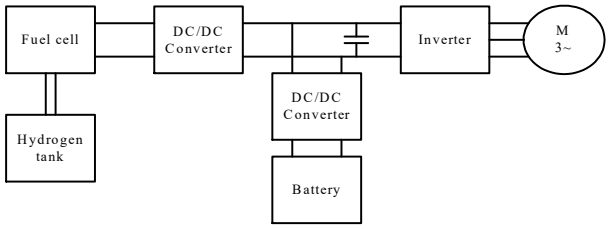

Fig. 1. Schematic representation of the traditional power train of a hydrogen train with fuel cells and batteries.

of energy storage of the boost DC-DC converters. Therefore, alternative topologies based on single-stage power converters could offer a more compact and power-dense solution. Open-ended winding induction machines could be used for this, with 2 separate inverters connected to the windings and fed by fuel cells and batteries, respectively [10]. This paper aims at assessing the potential to reduce the total apparent power of the power converters in comparison to a double-stage system.

The technical literature has presented mainly three different topologies for open-ended winding induction machines: dual inverters with one common power source; 2 isolated power sources; and one inverter with a power source and one inverter with a floating bridge [11], [12].

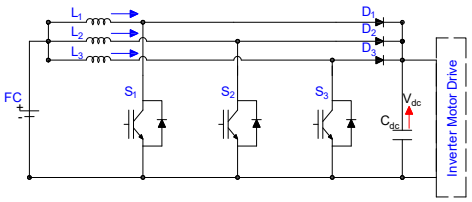

Fig. 2. Interleaved boost DC-DC converter of fuel cell

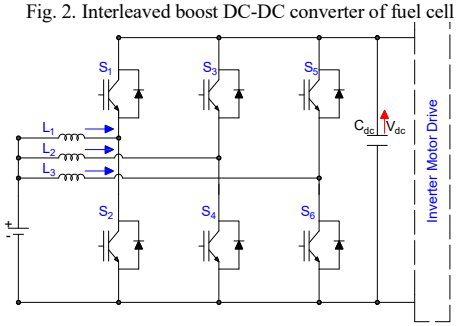

Fig. 3. Three-phase bi-directional DC-DC converter of battery

The main drawback of a dual inverter with a common power source is the need to suppress the zero-sequence component with isolation transformers [13]. However, some work has shown how specialised SWPVM techniques allow the suppression of this current component and, hence, remove the need for transformers [14]. Single power supply with common mode elimination [14],[15] also has been done in the literature using one additional leg, filters, and common mode choke, but more hardware is added into the scheme [16], [17].

The main drawback of the floating bridge is the capacitor voltage regulation. This application has been studied mostly for supplying the reactive power to the machine and then reducing the current and the power losses of the main inverter [18],[19],[20],[21]. In this topology, the floating inverter voltage must be controlled to be in quadrature with the motor current [22].

Substantial studies have been carried out to understand the best modulation strategies for open-ended winding induction machines. Initial work has been done using sine-triangle pulse width modulation (SPWM) [11], followed by several types of space-vector pulse width modulation (SVPWM) with the specific goal of understanding the possibility of obtaining a multilevel voltage waveform for the motor [14], [23], [24], [25], [26]. In fact, when the supply voltages of the 2 inverters are the same (e.g. both equal to $V_{dc}/2$) the motor voltage has three-level [11], [13]. When instead one of the 2 power sources has a voltage double of the other (e.g. 2/3 V_{dc} and 1/3 V_{dc}) a four-level voltage waveform is obtained [27]. When compared to other multilevel inverters, it has low switching losses with a moderate power circuit complexity [11], [28].

When 2 isolated power sources are available, like in the case of hydrogen trains, the dual inverter provides a higher degree of flexibility and has been chosen for this study. This configuration is also fault-tolerant in case of faults in any of the 2 inverters, as the 2 power sources can be used independently, albeit at lower voltages [29]. A modulation technique to balance power between the two inverters has been proposed in [30] and is considered in this study. The paper is organised as follows: the model and dynamic equations of the open-ended induction machine and power flow control techniques are given in section II. The design of the active and reactive powers of the inverters are explained in detail in section III. Then a discussion about the limitations of the dual inverter system for the specific case of hydrogen trains is reported in section IV. Finally, the conclusions are given in section V.

II. MODEL OF OPEN-ENDED WINDING INDUCTION MOTORS

The schematic of the dual two-level inverter scheme is shown in Fig. 4 with two isolated sources. The fuel cell is the primary energy source, while the battery provides the power peaks for the accelerations. While researchers have so far mainly focussed on the floating capacitor bridge, this paper uses both fuel cells and batteries to provide active and reactive power to the motor.

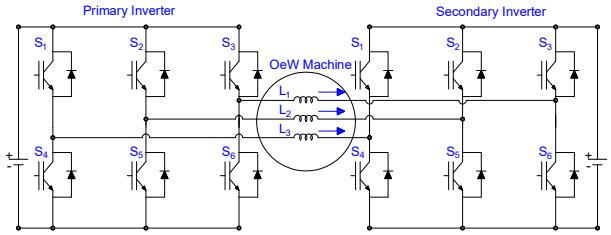

Fig. 4. Dual inverter fed open-ended winding induction motor topology.

Also, the primary inverter can be used to transfer active power to the secondary inverter via the machine windings, thereby offering the possibility of charging the battery both when the drive is motoring and braking.

A. Dynamic equations of open-ended induction motors

The dynamic mathematical model of open-ended induction machines is given by the following equations in the synchronous reference frame with rotor field-oriented control:

$$\begin{cases} \boldsymbol{v}_s = r_s \boldsymbol{i}_s + j\omega\sigma_s L_s \boldsymbol{i}_s + j\omega k_r \Phi_r + \sigma_s L_s \dfrac{d\boldsymbol{i}_s}{dt} + k_r \dfrac{d\Phi_r}{dt} \\ 0 = \sigma_r L_m \boldsymbol{i}_s + \sigma_r \Phi_r + j(\omega - p\omega_r)\Phi_r + \dfrac{d\Phi_r}{dt} \\ T_{el} = \dfrac{3}{2} p k_r \Phi_r \Im m\{\boldsymbol{i}_s\} \end{cases} \quad (1)$$

where $\boldsymbol{v}_s$ is the stator voltage space vector, $\boldsymbol{i}_s$ is the stator current space vector, Φ_r is the rotor flux linkage, T_{el} is the electromagnetic torque, r_s is the stator winding resistance, ω is the speed of the rotor flux linkage, p is the number of pole pairs, ω_r is the rotor speed, L_s is the total stator inductance, $k_r = L_m/L'_r$, where L_m is the motor self-inductance and L'_r is the rotor total inductance referred to a stator phase, $\sigma_r = r'_r / L'_r$, where r'_r is the rotor resistance referred to a stator phase, and $\sigma_s = 1 - L_m^2 / L_s L'_r$.

Standard field-oriented control is adopted up to the rated speed of the motor. For traction drives, the speed range is normally increased by adopting field-weakening, which is implemented by increasing the supply frequency at constant motor voltage [11].

For open-ended winding induction motors, the motor phase voltage can be calculated from the space vectors of the pole voltages of each inverter:

$$\boldsymbol{v}_s = \boldsymbol{v}_{s,fc} - \boldsymbol{v}_{s,b} \tag{2}$$

where $\boldsymbol{v}_{s,fc}$ is the space vector of the fuel cell inverter, $\boldsymbol{v}_{s,b}$ is the space vector of the voltage of the battery [7].

B. Power flow control techniques

The PWM is used to control the amplitude and phase of the fundamental component of the output voltage of the fuel cell and battery inverters so that the amplitude and phase of the motor voltage are controlled according to (2). Since the motor current is shared by the 2 inverters, the power sourced (or sinked) by each inverter is regulated by controlling the output voltage and phase produced by each inverter. The power split between the 2 inverters is defined by a higher-level vehicle system controller that regulates the power of the fuel cell and/or the state of charge of the battery [31].

The power split between the fuel cell and the battery is determined in three different ways. The total power delivered to the load, neglecting converter and motor losses, is given as:

$$P_m = P_{fc} + P_b \tag{3}$$

where P_m, $P_{fc,}$ and P_b are the load power, fuel cell power, and battery power, respectively. Using the induction motor model in (1) and the relation between motor voltage and inverters' voltages in (2), (3) becomes:

$$P_m = \frac{3}{2}\Re e\left\{\left(\boldsymbol{v}_{fc} - \boldsymbol{v}_b\right)\breve{\boldsymbol{i}}_s\right\} \tag{4}$$

The first method to control the power split is to operate the battery inverter with a unity power factor while controlling its output voltage amplitude [31]. This reduces the apparent power of the battery's inverter, while increasing the apparent power of the fuel cell's inverter and can be a convenient choice if there is a significant difference between the power split of the 2 sources. As a result, the fuel cell's inverter operates as a slack bus and it must supply the power to the motor, the battery, and all power losses.

The second method is when the fuel cell supplies the motor alone. Therefore, the battery is not used and this can be achieved by simply closing all three upper or lower switches in the battery's inverter to create a Y-connection of the stator windings. While this eliminates switching losses of the battery's converter, it also limits the voltage applied to the motor. As a result, this operating mode is only possible at low speeds. However, it is possible to increase the available motor voltage by controlling the battery's inverter with a voltage in quadrature with the motor current, as shown in [18]. Essentially, the battery's converter provides all the reactive power of the motor, while the fuel cell provides all the active power. This mode of operation is limited by the power factor of the motor, and it is more effective when the power factor is low, i.e. at low loads.

The third control mode is called optimum voltage control and it is achieved when the two inverters generate their voltages with opposite phase angles where the output voltages of the inverters are co-linear. As a result, required voltages are simply proportional to the desired power.

III. Design of Powers of the Inverter Units

A. Apparent power required by the motor drive

For vector-controlled motor drives, the current is controlled to generate a constant torque up to the base speed, and a constant power above the base speed. This is achieved by regulating the rotor flux linkage to the nominal level below the base-speed and then using field-weakening above the base-speed to keep the motor voltage at the nominal value. An example of a real motor with a power of 11 kW is shown in Fig.5. As well-known, the maximum apparent power of the motor is obtained at the base speed (in the example, S_{max} = 15.4 kVA, P_{max} = 12.7 kW, Q_{max} = 8.8 kvar). Above the base-speed, the apparent power is constant because both the voltage and the current are limited to their nominal values [13]. Therefore, the base speed can be used for the design of the apparent power of the inverters, whereas the switching frequency should be chosen as a trade-off between inverter losses and the quality of the current at the maximum speed. For standard machines, the design of the apparent power of the inverter is straightforward, as it is equal to the apparent power of the motor augmented by the inverter losses. Similarly, the apparent power of the DC-DC converters can be calculated from the voltage of the DC-bus and the maximum current of the fuel cell and the battery. Conversely, for open-ended winding machines, the motor power is fed by the 2 inverters and it is necessary to ensure that the total apparent power of the 2 inverters is minimised.

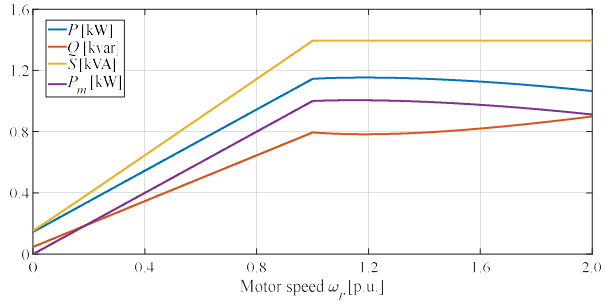

Fig. 5. Powers of a vector controlled open-winding machines below and above the base speed (values in per unit of the nominal power).

B. Design of the minimum apparent power when the fuel cell and battery are both supplying the motor

For open-ended winding machines, the total apparent power of the inverters, S_{tot}, is equal to:

$$S_{tot} = S_{fc} + S_b = \sqrt{P_{fc}^2 + Q_{fc}^2} + \sqrt{P_b^2 + Q_b^2} \tag{5}$$

being S_{fc} and S_b the apparent powers of the fuel cell and battery inverters, P_{fc} and P_b their active powers, and Q_{fc} and Q_b their reactive powers, respectively. Also, we can write the following inequalities:

$$\begin{cases} P_{fc} + P_b = P_{tot} \le P_{max} \\ Q_{fc} + Q_b = Q_{tot} \le Q_{max} \end{cases} \tag{6}$$

where P_{max} and Q_{max} are the maximum active and reactive powers of the machine as indicated in Fig. 1. By using these maximum powers and substituting (6) into (5), we obtain:

$$S_{tot} = \sqrt{P_{fc}^2 + Q_{fc}^2} + \sqrt{\left(P_{max} - P_{fc}\right)^2 + \left(Q_{max} - Q_{fc}\right)^2} \tag{7}$$

This equation can be seen as a function of the 2 variables P_1 and Q_1 and it can be seen if they have any minima by looking at the stationary points:

$$\begin{aligned}\frac{\partial S_{tot}}{\partial P_{fc}} &= \frac{P_{fc}}{\sqrt{P_{fc}^2+Q_{fc}^2}} - \frac{P_{\max}-P_{fc}}{\sqrt{\left(P_{\max}-P_{fc}\right)^2+\left(Q_{\max}-Q_{fc}\right)^2}} = 0 \\ \frac{\partial S_{tot}}{\partial Q_{fc}} &= \frac{Q_{fc}}{\sqrt{P_{fc}^2+Q_{fc}^2}} - \frac{Q_{\max}-P_{fc}}{\sqrt{\left(P_{\max}-P_{fc}\right)^2+\left(Q_{\max}-Q_{fc}\right)^2}} = 0\end{aligned} \tag{8}$$

These 2 equations are both satisfied when:

$$\begin{cases}\dfrac{P_{fc}}{P_{\max}} = \dfrac{Q_{fc}}{Q_{\max}} \\ \dfrac{P_b}{P_{\max}} = 1-\dfrac{P_{fc}}{P_{\max}} = 1-\dfrac{Q_{fc}}{Q_{\max}}\end{cases} \tag{9}$$

The minimum condition can be verified by substituting the stationary points in the Hessian determinant and verifying that the minors of this matrix have the same sign of the determinant (not included here for brevity). Equations (9) shows that the minimum apparent power is obtained when the 2 inverters are loaded in the same proportions in terms of active and reactive powers at the base speed and above. With this selection, the minimum total apparent power of the 2 inverters is:

$$S_{tot,\min} = Q_{fc}\sqrt{\frac{P_{\max}^2}{Q_{\max}^2}+1} + \left(Q_{\max}-Q_{fc}\right)\sqrt{\frac{P_{\max}^2}{Q_{\max}^2}+1} = \sqrt{P_{\max}^2+Q_{\max}^2} \tag{10}$$

and hence equal to the apparent power of a single inverter feeding a traditional motor (i.e. not open-ended). That means that at least in principle, the open-ended configuration requires 50% apparent power of the configuration in Fig. 1. Additionally, below the base speed there is a degree of freedom on how to split the active and reactive powers assigned to the 2 inverters.

C. *Power split strategy during train acceleration*

Due to power losses, it is important to decide how to split the active and reactive powers of the 2 inverters. In the open-winding configuration, the inverters share the same ac current, while the voltage depends on the power. Therefore, as the fuel cell provides the base load, it is convenient to use the fuel cell converter as much as possible, at least up to the level for which the motor requires a power higher than that available from the fuel cell. In particular, 2 strategies can be devised based on whether the fuel cell is asked also to charge the battery during train acceleration. If the battery is not being charged (Fig. 4), then the fuel cell can be used alone at low speed, so that the battery converter is not switching and it is kept in short-circuit mode. This has an implication in the number of available levels of the motor voltage, but this is not typically a problem, as at low speed the motor voltage is also low. Assuming the max active and reactive powers of the fuel cell converter are equal to 50% of the max values, the apparent power of the converter would be 46% of the maximum apparent power of the motor. Looking at Fig. 6, drawn at nominal motor current, that means that for speeds up to 40% of the rated value, the converter of the fuel cell can handle both the active and the reactive powers of the motor. Above that speed, the fuel cell converter is used at its maximum power level, while the battery converter is activated and covers the residual power requirements. The curves will be simply scaled for currents

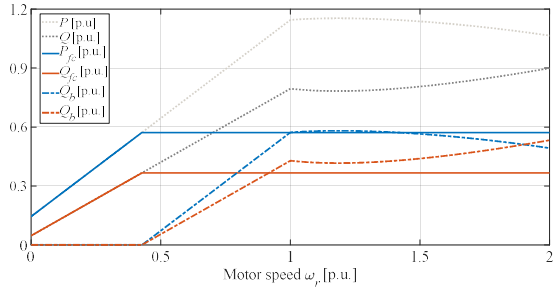

Fig. 6. Optimal power split when the fuel cell does not charge the battery during train acceleration.

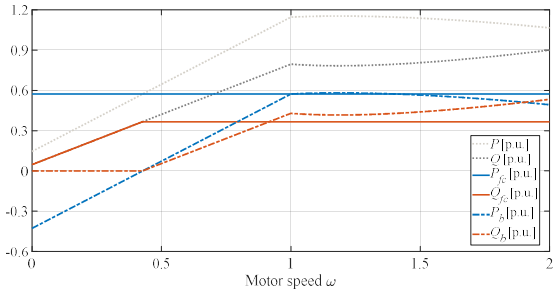

Fig. 7. Optimal power split when the fuel cell charges the battery during train acceleration.

lower than the nominal, as the limiting factor of the power sharing is the voltage for an open-ended machine.

If the battery is also charged during the train's acceleration (Fig. 7), then the fuel cell converter is used at its rated active power from the standstill, while the reactive power follows the motor requirement. That means that the battery converter must operate at a unity power factor, albeit negative, to enable the power transfer to the battery. The available charging power decreases with the speed, as some of it must be used for the motor. Above the speed of 40% of the rated value, the fuel cell cannot charge the battery at all, at least as long as the acceleration phase is not over. Considering the limited time for a train acceleration, usually under a few minutes, it might not be worth using this mode at all.

IV. Design of the Minimum Apparent Power to Charge the Battery from the Fuel Cell

From the previous analysis, it is clear that the design of the 2 converters depends on the fraction of active power that the fuel cell provides to the motor. To reduce the fuel cell size, this is typically limited to the average power required in the traction cycle, which is normally approximately 40-45% of the peak power, augmented by a safety margin to take into account power losses and other effects not captured by the models. However, as the 2 inverters share the same current, reduced apparent power of the fuel cell converter means reduced maximum voltage output. This can be a limitation if the fuel cell is required to charge the battery when the train travels at a high speed, as the motor voltage will be high, and it will not be possible to select a voltage vector for the battery inverter that ensure a negative power factor. This can be easily seen from the vector diagrams of Fig. 8, which have been drawn at the motor's rated speed and for a maximum fuel cell voltage equal to 50% of the nominal motor voltage.

When the current is equal to the nominal value, the power factor of the motor is high and hence the projection of the motor voltage $\boldsymbol{V}_m$ on the current vector $\boldsymbol{I}_m$ is larger than the

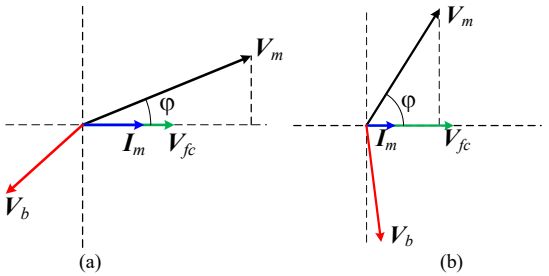

Fig. 8. Vector diagram for base speed and motor current equal to nominal (a) or 50% of the nominal (b).

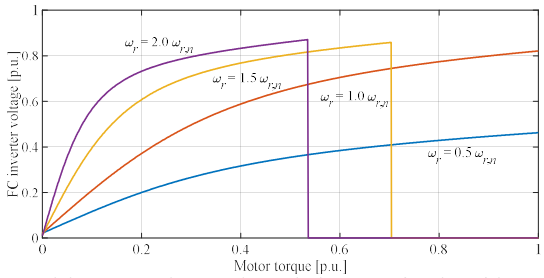

Fig. 9. Minimum FC voltage to charge the battery as function of the motor torque for different motor speeds.

fuel cell voltage, even if $\boldsymbol{V}_{fc}$ is aligned with the current, as shown in Fig. 8a. Therefore, the fuel cell cannot charge the battery, as the angle of $\boldsymbol{V}_b$ can't be larger than 90 degrees.

If instead, the current is lower than the nominal, for example, 50%, then the power factor is much lower, as the reduction of the current is fully due to the reduction of the quadrature component i_{sq} as the flux linkage is maintained constant. As such, the projection of $\boldsymbol{V}_m$ on $\boldsymbol{I}_m$ can be smaller than $\boldsymbol{V}_{fc}$ and then the fuel cell can charge the battery. Assuming the motor current as the reference for the phase, i.e. $\boldsymbol{I}_m = |\boldsymbol{I}_m|$, the following equations can be derived:

$$\boldsymbol{V}_b = |\boldsymbol{V}_{fc}| - |\boldsymbol{V}_m|\cos\varphi - j|\boldsymbol{V}_m|\sin\varphi \tag{11}$$

therefore, the power that can be used to charge the battery depends on the difference between the maximum fuel cell voltage and the projection of the motor voltage:

$$P_b = \Re e\left\{\boldsymbol{V}_b\,\breve{\boldsymbol{I}}_m\right\} = \left(|\boldsymbol{V}_{fc}| - |\boldsymbol{V}_m|\cos\varphi\right)|\boldsymbol{I}_m| \tag{12}$$

To ensure this power is charging the battery, the fuel cell's maximum voltage must be designed with a sufficient margin. This margin can be obtained from the mathematical model of induction machines with vector control using as input the torque T_{el} required by the motor:

$$|\boldsymbol{V}_{fc}| > |\boldsymbol{V}_m|\cos\varphi = r_s|\boldsymbol{I}_m| + \frac{\omega}{|\boldsymbol{I}_m|}\frac{2T_{el}}{3p} \tag{13}$$

and, assuming now the total rotor flux linkage as the reference for the phase:

$$\begin{aligned} \boldsymbol{I}_m &= i_{sd} + j\frac{2T_{el}}{3p}\frac{L_r'}{L_m^2}\frac{1}{i_{sd}} \\ \omega &= p\omega_r + \frac{2T_{el}}{3p}\frac{r_r'}{L_m^2}\frac{1}{i_{sd}^2} \end{aligned} \tag{14}$$

where the direct axis component of the current is:

$$i_{sd} = \begin{cases} i_{sd,n} & \omega_r \le \omega_{r,n} \\ i_{sd,n}\dfrac{\omega_{r,n}}{\omega_r} & \omega_r > \omega_{r,n} \end{cases} \tag{15}$$

where $i_{sd,n}$ and $\omega_{r,n}$ are the rated values of the direct axis current and speed, respectively. These equations point out that the minimum voltage of the fuel cell inverter to charge the battery depends on the motor speed and torque, as shown in Fig. 9, where the curves above the rated speed can be drawn up to a maximum torque value given by the field weakening, i.e. roughly the nominal power divided by the speed.

This figure highlights that for higher speeds, a higher voltage is required, albeit with a less than linear increment. This is because the quadrature component of the current increases more than the reduction of the direct component, resulting in a higher current magnitude. As the voltage remains constant in field-weakening, the power factor increases only slightly. For typical traction cycles, assuming the top speed equal to twice the rated value, the steady-state torque of the motor is in the range of 0.2-0.3 p.u., which means that a voltage of 0.7-0.8 p.u. is required by the fuel cell inverter to charge the battery up to the top-speed. Therefore, if the fuel cell and the battery both supply up to 50% of the motor power, it results that the minimum apparent power of the topology is roughly 1.3 times the apparent power of the motor, i.e. approximately 65% lower than the value required by the topology in Fig. 1.

One of the concerns of this topology is charging the battery while the train is stationary. This is not an issue, as the vector control can require zero torque at zero speed and all the current is magnetising at zero frequency. The only problem is that the motor is saturated because the component i_d is higher than the nominal value, so it is important to check if the current ripple is acceptable because of the lower inductance.

V. Conclusions

This study has undertaken an analytical investigation of the control principles of open-ended winding induction machines for railway traction fed by fuel cells and batteries. The results show that this configuration can achieve a reduction of up to 65% of the total apparent power of the power converters, as the DC/DC converters are eliminated in comparison with the state-of-the-art solution. The main limitation of this traction circuit is the voltage of the fuel cell which needs to be sufficiently high to charge the battery at high speeds, which is a situation currently occurring in hydrogen trains. However, the low motor torque of the motor when the train is cruising results in a lower motor power factor that partially mitigates the required magnitude of the fuel cell voltage. This problem can be solved using a fuel cell with a higher voltage and with an overdesign of the fuel cell converter, albeit this reduces the advantage of the proposed solution in comparison with a standard configuration that will be investigated further in future studies, together with a detailed analysis of the power losses.

VI. References

[1] D. Kang, S. Yun, and B. K. Kim, "Review of the Liquid Hydrogen Storage Tank and Insulation System for the High-Power Locomotive," *Energies*, vol. 15, no. 12. MDPI, Jun. 01, 2022. doi: 10.3390/en15124357.

[2] K. Mazloomi and C. Gomes, "Hydrogen as an energy carrier: Prospects and challenges," *Renewable and Sustainable Energy Reviews*, vol. 16, no. 5. pp. 3024–3033, Jun. 2012. doi: 10.1016/j.rser.2012.02.028.

[3] M. Haji Akhoundzadeh, S. Panchal, E. Samadani, K. Raahemifar, M. Fowler, and R. Fraser, "Investigation and simulation of electric train utilizing hydrogen fuel cell and lithium-ion battery," *Sustainable Energy Technologies and Assessments*, vol. 46, Aug. 2021, doi: 10.1016/j.seta.2021.101234.

[4] X. Chang, T. Ma, and R. Wu, "Impact of urban development on residents' public transportation travel energy consumption in China: An analysis of hydrogen fuel cell vehicles alternatives," *Int J Hydrogen Energy*, pp. 16015–16027, Jun. 2019, doi: 10.1016/j.ijhydene.2018.09.099.

[5] A. Hoffrichter, S. Hillmansen, and C. Roberts, "Conceptual propulsion system design for a hydrogen-powered regional train," *IET Electrical Systems in Transportation*, vol. 6, no. 2, pp. 56–66, Jun. 2016, doi: 10.1049/iet-est.2014.0049.

[6] M. İnci, M. Büyük, M. H. Demir, and G. İlbey, "A review and research on fuel cell electric vehicles: Topologies, power electronic converters, energy management methods, technical challenges, marketing and future aspects," *Renewable and Sustainable Energy Reviews*, vol. 137. Elsevier Ltd, Mar. 01, 2021. doi: 10.1016/j.rser.2020.110648.

[7] H. S. Das, C. W. Tan, and A. H. M. Yatim, "Fuel cell hybrid electric vehicles: A review on power conditioning units and topologies," *Renewable and Sustainable Energy Reviews*, vol. 76. Elsevier Ltd, pp. 268–291, 2017. doi: 10.1016/j.rser.2017.03.056.

[8] N. Benyahia *et al.*, "MPPT controller for an interleaved boost dc-dc converter used in fuel cell electric vehicles," *Int J Hydrogen Energy*, vol. 39, no. 27, pp. 15196–15205, Sep. 2014, doi: 10.1016/j.ijhydene.2014.03.185.

[9] M. Kabalo, B. Blunier, D. Bouquain, and A. Miraoui, State-of-the-Art of DC-DC Converters for Fuel Cell Vehicles.

[10] E. Fedele, D. Iannuzzi, P. Tricoli, and A. del Pizzo, "NPC-based Multi-Source Inverters for Multimode DC Rail Traction Systems," *IEEE Transactions on Transportation Electrification*, 2022, doi: 10.1109/TTE.2022.3175097.

[11] "Configurations_of_high-power_voltage_source_inverter_drives".

[12] Z. Huang, T. Yang, P. Giangrande, M. Galea, and P. Wheeler, "Technical Review of Dual Inverter Topologies for More Electric Aircraft Applications," *IEEE Transactions on Transportation Electrification*, vol. 8, no. 2, pp. 1966–1980, Jun. 2022, doi: 10.1109/TTE.2021.3113606.

[13] M. R. Baiju, K. K. Mohapatra, R. S. Kanchan, and K. Gopakumar, "A dual two-level inverter scheme with common mode voltage elimination for an induction motor drive," *IEEE Trans Power Electron*, vol. 19, no. 3, pp. 794–805, May 2004, doi: 10.1109/TPEL.2004.826514.

[14] K. A. Corzine, M. W. Wielebski, F. Z. Peng, and J. Wang, "Control of cascaded multilevel inverters," *IEEE Trans Power Electron*, vol. 19, no. 3, pp. 732–738, May 2004, doi: 10.1109/TPEL.2004.826495.

[15] B. R. Vinod and M. R. Baiju, "Direct torque control implemented on a three-level open-end winding induction motor drive," in *IEEE International Conference on Power Electronics, Drives and Energy Systems, PEDES 2016*, Apr. 2017, vol. 2016-January, pp. 1–6. doi: 10.1109/PEDES.2016.7914353.

[16] V. T. Somasekhar, K. Gopakumar, M. R. Baiju, K. K. Mohapatra, and L. Umanand, "A multilevel inverter system for an induction motor with open-end windings," *IEEE Transactions on Industrial Electronics*, vol. 52, no. 3, pp. 824–836, Jun. 2005, doi: 10.1109/TIE.2005.847584.

[17] K. Ramachandrasekhar, S. Mohan, and S. Srinivas, "An improved PWM for a dual two-level inverter fed open-end winding induction motor drive," in *19th International Conference on Electrical Machines, ICEM 2010*, 2010. doi: 10.1109/ICELMACH.2010.5607866.

[18] E. G. Shivakumar, K. Gopakumar, S. K. Sinha, A. Pittet, and V. T. Ranganathan, "Space vector PWM control of dual inverter fed open-end winding induction motor drive," in *Conference Proceedings - IEEE Applied Power Electronics Conference and Exposition - APEC*, 2001, vol. 1, pp. 399–405. doi: 10.1109/apec.2001.911678.

[19] J. Kalaiselvi, K. Rama Chandra Sekhar, and S. Srinivas, "Common mode voltage elimination PWMs for a dual two-level VSI with single inverter switching," in *IEEE International Symposium on Industrial Electronics*, 2012, pp. 234–239. doi: 10.1109/ISIE.2012.6237090.

[20] A. L. Julian, G. Oriti, and T. A. Lipo, "Elimination of common-mode voltage in three-phase sinusoidal power converters," *IEEE Trans Power Electron*, vol. 14, no. 5, pp. 982–989, 1999, doi: 10.1109/63.788504.

[21] Y. C. Son and S. K. Sul, "A New Active Common-Mode EMI Filter for PWM Inverter," *IEEE Trans Power Electron*, vol. 18, no. 6, pp. 1309–1314, Nov. 2003, doi: 10.1109/TPEL.2003.818829.

[22] J. Kim, J. Jung, and K. Nam, "Dual-inverter control strategy for high-speed operation of EV induction motors," *IEEE Transactions on Industrial Electronics*, vol. 51, no. 2, pp. 312–320, Apr. 2004, doi: 10.1109/TIE.2004.825232.

[23] J. Ewanchuk, J. Salmon, and C. Chapelsky, "A method for supply voltage boosting in an open-ended induction machine using a dual inverter system with a floating capacitor bridge," *IEEE Trans Power Electron*, vol. 28, no. 3, pp. 1348–1357, 2013, doi: 10.1109/TPEL.2012.2207741.

[24] R. U. Haque, A. Kowal, J. Ewanchuk, A. Knight, and J. Salmon, "PWM control of a dual inverter drive using an open-ended winding induction motor," in *Conference Proceedings - IEEE Applied Power Electronics Conference and Exposition - APEC*, 2013, pp. 150–156. doi: 10.1109/APEC.2013.6520200.

[25] C. Perera, G. J. Kish, and J. Salmon, "Decoupled Floating Capacitor Voltage Control of a Dual Inverter Drive for an Open-Ended Winding Induction Motor," *IEEE Trans Power Electron*, vol. 35, no. 7, pp. 7305–7316, Jul. 2020, doi: 10.1109/TPEL.2019.2955412.

[26] E. G. Shivakumar, V. T. Somasekhar, K. K. Mohapatra, K. Gopakumar, L. Umanand, and S. K. Sinha, "A multi level space phasor based PWM strategy for an open-end winding induction motor drive using two inverters with different DC link voltages," in *Proceedings of the International Conference on Power Electronics and Drive Systems*, 2001, vol. 1, pp. 169–175. doi: 10.1109/peds.2001.975306.

[27] B. Venugopal Reddy, V. T. Somasekhar, and Y. Kalyan, "Decoupled space-vector PWM strategies for a four-level asymmetrical open-end winding induction motor drive with waveform symmetries," *IEEE Transactions on Industrial Electronics*, vol. 58, no. 11, pp. 5130–5141, Nov. 2011, doi: 10.1109/TIE.2011.2116759.

[28] K. Safsouf, J. Sawma, and H. Y. Kanaan, "A Comparative Study of Open-End Winding Drive Systems for Hybrid Fuel Cell-Battery Fed Electric Vehicles," in *2021 IEEE 3rd International Multidisciplinary Conference on Engineering Technology, IMCET 2021*, 2021, pp. 49–54. doi: 10.1109/IMCET53404.2021.9665621.

[29] M. R. Baiju, K. K. Mohapatra, R. S. Kanchan, and K. Gopakumar, "A dual two-level inverter scheme with common mode voltage elimination for an induction motor drive," *IEEE Trans Power Electron*, vol. 19, no. 3, pp. 794–805, May 2004, doi: 10.1109/TPEL.2004.826514.

[30] G. Grandi and D. Ostojic, "Dual inverter space vector modulation with power balancing capability," in *IEEE EUROCON 2009, EUROCON 2009*, 2009, pp. 721–728. doi: 10.1109/EURCON.2009.5167713.

[31] J. Kim, J. Jung, and K. Nam, "Dual-inverter control strategy for high-speed operation of EV induction motors," *IEEE Transactions on Industrial Electronics*, vol. 51, no. 2, pp. 312–320, Apr. 2004, doi: 10.1109/TIE.2004.825232.

[32] M. R. Baiju, K. K. Mohapatra, R. S. Kanchan, and K. Gopakumar, "A dual two-level inverter scheme with common mode voltage elimination for an induction motor drive," *IEEE Trans Power Electron*, vol. 19, no. 3, pp. 794–805, May 2004, doi: 10.1109/TPEL.2004.826514.

[33] N. Ertugrul, W. Soong, G. Dostal, and D. Saxon, "Fault tolerant motor drive system with redundancy for critical applications," in *PESC Record - IEEE Annual Power Electronics Specialists Conference*, 2002, vol. 3, pp. 1457–1462. doi: 10.1109/psec.2002.1022381.

[34] A. Nabae, I. Takahashi, and H. Akagi, "A New Neutral-Point-Clamped PWM Inverter," *IEEE Trans Ind Appl*, vol. IA-17, no. 5, pp. 518–523, 1981, doi: 10.1109/TIA.1981.4503992.

[35] K. Ramachandrasekhar, S. Mohan, and S. Srinivas, "An improved PWM for a dual two-level inverter fed open-end winding induction motor drive," in *19th International Conference on Electrical Machines, ICEM 2010*, 2010. doi: 10.1109/ICELMACH.2010.5607866.

[36] B. A. Welchko, "A double-ended inverter system for the combined propulsion and energy management functions in hybrid vehicles with energy storage," in *IECON Proceedings (Industrial Electronics Conference)*, 2005, vol. 2005, pp. 1401–1406. doi: 10.1109/IECON.2005.1569110.